Chemical Engineering Journal 101 (2004) 225–235

Chemical Engineering Journal

www.elsevier.com/locate/cej

# Design of a molybdenum high throughput microreactor for high temperature screening of catalytic coatings

M.J.M. Mies, E.V. Rebrov, M.H.J.M. de Croon, J.C. Schouten*

*Department of Chemical Engineering and Chemistry, Eindhoven University of Technology, P.O. Box 513, 5600 MB Eindhoven, The Netherlands*

**Abstract**

This paper focuses on a CFD approach to optimize the design parameters for a high throughput microreactor prior to reactor micromachining and assembling. A molybdenum-based microreactor has been designed for the screening of catalytic coatings in the 100–800 °C temperature range in gas phase reactions involving large heat effects ($\Delta H_{298} = \pm 500$ kJ/mol). The microreactor consists of eight microstructured compartments, each with a cross section of 2.28 mm × 10.18 mm and 40 mm in length. Eight 100 μm thick molybdenum plates with a deposited catalytic layer with a thickness up to 10 μm are to be inserted in each compartment at distances of 130 μm from each other. Using the CFD code Fluent®6.0, it is demonstrated that a low-pressure drop flow diffuser, positioned upstream of the microreactor, distributes reactants evenly in a flow range of 50–1000 $cm^3$/min (STP) throughout all compartments. The gas sampling section allows to analyse the reaction products from a selected compartment with no interference from adjacent compartments. The quench section provides a fast quench of the effluent gases within milliseconds to avoid consecutive reactions. The corrosion resistance of the reactor can be improved by atomic layer deposition of a 200 nm α alumina layer.


*Keywords:* CFD approach; Molybdenum; Microreactor; Catalytic coating; High throughput

## 1. Introduction

In the overall optimal design of a catalytic process, the choice of the catalyst with its operating conditions is the critical step, which defines the costs of the reaction against the costs of product recovery and by-product treatment. For secondary screening of heterogeneous catalysts, there exist two types of reactor concepts: (1) multi-tubular fixed bed reactor modules, which closely resemble conventional catalyst testing apparatus, and (2) microreactor arrays, in which often catalyst coatings can be screened [1]. Table 1 presents the state-of-the-art in high throughput experimentation with respect to the secondary screening step, where heterogeneous catalysts can be optimized for gas phase reactions.

A major issue in the development of secondary gas phase screening reactors is to operate the whole device at the same conditions. However, flow non-uniformities up to 30% (Table 1) within one reactor system are common, which is often the result of an inadequate design of the flow diffuser. Furthermore, when the reactor is constructed of materials with a low thermal conductivity, temperature differences of about 5 K are reported already in absence of any catalytic reaction (Table 1). Even higher gradients are expected during reaction, especially when large heat effects are involved. Most of the reactors, besides those constructed of ceramics and quartz, have a maximum operating temperature around 550 °C, while numerous catalytic applications require temperatures higher than this. Furthermore, these devices are often made from materials with a relatively low thermal conductivity, so they cannot be applied to study the catalyst performance in reactions with high thermal effects. In order to realize such applications, new techniques have to be developed for producing microchannels, e.g. in refractory metals or aluminide intermetallics, which is a real challenge. In several catalytic processes, a potential for improving the overall performance exists by improving either the active component itself or the catalyst texture. Various examples are listed in Table 2.

In the development of a high throughput microreactor (HTMR) for high temperature applications (Table 2) several issues have to be considered such as material choice, reactor geometry, catalyst incorporation techniques, and microreactor fabrication methods. In this way, CFD simulations can provide detailed information on design parameters and reactor performance. This latter aspect is evident in order to overcome relatively large performance deviations, as summarized in Table 1 for existing screening systems. This non-ideality can apparently be attributed to a

* Corresponding author. Tel.: +31-40-247-2850; fax: +31-40-244-6653.
*E-mail address:* j.c.schouten@tue.nl (J.C. Schouten).

1385-8947/$ – see front matter © 2003 Elsevier B.V. All rights reserved.
doi:10.1016/j.cej.2003.11.024

**Nomenclature**

| | |
|---|---|
| $a$ | minimum length between two adjacent reactor compartment walls (m) |
| $b$ | minimum length between the top wall of the reactor compartment and a sidewall of a diffuser compartment (m) |
| $c$ | width of the reactor compartment, $c = 2.26 \times 10^{-3}$ m |
| $d$ | position of the capillary inlet inside a compartment (m) |
| $E$ | tension modulus (GPa) |
| $h$ | height of the diffuser compartment (m) |
| $\Delta H^{\circ}_{298}$ | heat of formation at 25 °C (kJ/mol) |
| $i$ | reactor compartment number, $1 \leq i \leq 4$ |
| $l$ | distance between a Mo plate and the main body of the raector |
| $Q$ | heat flux (W) |
| $s$ | mean square deviation from the average flow value |
| $S$ | cross section area, four times the distance in which the plates are inserted inside the microstructure ($4 \times 0.2$ mm) times the reactor length (40 mm), $S = 3.2 \times 10^{-5}$ m$^2$ |
| $T$ | temperature (°C) |
| $T_{\text{melt}}$ | melting temperature of material (°C) |
| $\Delta T$ | temperature difference (K) |
| $u_i$ | area averaged velocity in the compartment $i$ |
| $\bar{u} = \frac{1}{4}\sum_{i=1}^{4} u_i$ | The average flow value in the four compartments considered for simulation |
| *Greek letters* | |
| $\alpha$ | linear extension coefficient (K$^{-1}$) |
| $\delta$ | flow non-uniformity (%) |
| $\lambda$ | heat conductivity coefficient (W m$^{-1}$ K$^{-1}$) |

point of controversy between an experimental-based and a simulation-based reactor development approach.

Lack of data for application of an HTMR in high temperature reactions with large heat effects prompted us to study the behaviour of this system using the CFD code Fluent®6.0. Therefore, this paper focuses on a CFD approach in order to show the importance of reactor design through simulation prior to experimentation. A design methodology covers three essential issues for the application of an HTMR. A flow diffuser is designed to provide equal contact times in the separate reactor compartments, while the intrinsic features of the microreactor geometry and material should provide near-isothermal conditions. Secondly, to achieve results with high accuracy, the products from one compartment should be analysed with no interference from products from adjacent compartments. Finally, the quench section has to quench the effluent flow within a millisecond range to avoid consecutive non-catalytic reactions.

## 2. Development of a high throughput microreactor

### 2.1. Geometry and material choice

Microstructured plate-type reactors can be effectively used for testing of catalytic coatings. A large number of plates, on which the catalyst coating is deposited, can be efficiently utilized within the micrometer range. In this way, a relatively high surface area available to the reactants can be obtained. Furthermore, microstructured reactors with adequate characteristics and dimensions guarantee negligible pressure drop and the absence of external diffusion limitations in the whole range of reaction conditions [28,29]. Near-isothermal reactor operation can be realized in a plate-type microreactor by the effective dissipation of reaction heat by a proper choice of thermal conductivity and geometry of the plate material and the reactor [28–31]. Table 3 presents the physical data of various materials from which (micro) reactors are or can be manufactured.

It is clear that only a limited number of materials can be used at elevated temperatures, because of a relatively low melting point, e.g. aluminium and copper, or of a rather low mechanical stability, e.g. quartz and nickel. A further selection of reactor material is based on the thermal conductivity, which narrows the choice of material to silicon and some of the refractory metals. Silicon, however, has several drawbacks as low wettability of the surface, which limits its application as substrate for catalytic coatings, and a low fracture toughness, which makes its application as basic reactor material unfeasible. On the contrary, several refractory metals satisfy all design criteria, which enables its application in high temperature processes involving large heat effects. In the design of the high throughput microreactor, molybdenum was chosen as basic reactor material as well as material for parallel plates, eliminating construction problems relating to compatibility of different materials at elevated temperatures.

The HTMR was designed to test eight different catalytic coatings with a maximum thickness of 10 μm, which are deposited on molybdenum plates of 40 mm length, 10 mm width, and 0.1 mm thickness, and to operate at a minimal reaction rate of $5 \times 10^{-3}$ s$^{-1}$ in terms of turnover frequency (TOF). The reactor consists of eight identical microstructured compartments (Fig. 1). This arbitrary chosen number of compartments can be increased when this specific reactor concept is proven to operate adequately. Eight molybdenum plates with deposited catalytic coatings are inserted in each compartment. In this way, a total number of 64 molybdenum plates are stacked in the HTMR to screen eight different catalytic coating compositions simultaneously. If necessary, both the coating thickness and the total area of the substrate can be easily changed to operate the HTMR in

Table 1
Secondary gas phase screening reactors reported in literature; reactor characteristics, and applied model reactions and reaction conditions

| Reactor characteristics | | | | | Process characteristics | | | Ref. |
|---|---|---|---|---|---|---|---|---|
| Material + ($\Delta T$)[a] without reaction | Mode[b] | No.[c] | $\delta$[d] (%) | $T$ (°C) | Reaction | Catalyst system/library | $\Delta H^{\circ}_{298}$ (kJ/mol) | |
| Multi-tubular reactors | | | | | | | | |
| Quartz (n.d.[e]) | D/I | 6 | n.d. | 250 | $CO + \frac{1}{2}O_2 \rightarrow CO_2$ | Cu–Cr/active carbon | −283 | [2] |
| | | | | 600 | $N_2O \rightarrow N_2 + \frac{1}{2}O_2$ | Fe-ZSM-5 | −83 | [2,3] |
| | | | | 150 | $NO + NH_3 + \frac{1}{4}O_2 \rightarrow N_2 + 1\frac{1}{2}H_2O$ | $Mn_2O_3$–$WO_3$/γ-$Al_2O_3$ | −407 | [2,4] |
| Brass (1) | I | 16 | n.d. | 180 | $CO + \frac{1}{2}O_2 \rightarrow CO_2$ | Au/$Co_3O_4$, Au/$TiO_2$ | −283 | [5] |
| Stainless steel (5) | I | 49 | 10 | 550 | $CH_4 + 2O_2 \rightarrow CO_2 + 2H_2O$ | Pt/$TiO_2$, Cu/$Al_2O_3$ | −802 | [6] |
| Quartz (5) | I | 10 | 30 | 700 | $CH_4 + CO_2 \rightarrow 2CO + 2H_2$ | Pt/$Ce_{1-x}Gd_xO_{2-0.5x}$, Pt/$Ce_{1-x}Sm_xO_{2-0.5x}$ | +247 | [7] |
| Alumina (5) | I | 64 | 7.5 | 550 | $C_2H_6 + \frac{1}{2}O_2 \rightarrow C_2H_4 + H_2O$ | Metal-oxides/α-$Al_2O_3$ | −106 | [8] |
| | | | | 500 | $C_3H_8 + \frac{1}{2}O_2 \rightarrow C_3H_6 + H_2O$ | Metal-oxides/α-$Al_2O_3$ | −117 | |
| Quartz (n.d.) | I | 15 | n.d. | 800 | $CH_4 + \frac{1}{4}O_2 \rightarrow \frac{1}{2}C_2H_6 + \frac{1}{2}H_2O$ | Mn–$Na_2WO_4$/$SiO_2$ | −88 | [9,10] |
| | | | | 200 | $C_3H_8 + 5O_2 \rightarrow 3CO_2 + 4H_2O$ | Multi-metal/$TiO_2$ | −2043 | [11] |
| | | | | 250 | $CO + \frac{1}{2}O_2 \rightarrow CO_2$ | Au/carrier | −283 | [9] |
| Microreactors | | | | | | | | |
| Ceramic (I) | D | 80 | 5 | 350 | $C_6H_{12} \rightarrow C_6H_6 + 3H_2$ | Pt–Pd–In/γ-$Al_2O_3$ | +206 | [12–14] |
| | I | | | 550 | $NO + C_3H_6 + 4O_2 \rightarrow$ | Pt–Pd–In–Na/γ-$Al_2O_3$ | −1838 | [12,15] |
| | | | | 250 | $\frac{1}{2}N_2 + 3CO_2 + 3H_2O$ | | | |
| | | | | | $C_3H_8 + 5O_2 \rightarrow 3CO_2 + 4H_2O$ | Multi-metal/$TiO_2$ | −2043 | [11,12] |
| Aluminium wafers/(n.d.) | I | 35 | 10 | 450 | $CH_4 + 2O_2 \rightarrow CO_2 + 2H_2O$ | Pt–Zr–V/γ-$Al_2O_3$ | −802 | [16–18] |
| Ceramic (5) | I | 256 | 10 | 450 | $CH_4 + 2O_2 \rightarrow CO_2 + 2H_2O$ | Pt–Zr–V/γ-$Al_2O_3$ | −802 | [18,19] |
| | | | | 250 | $CO + \frac{1}{2}O_2 \rightarrow CO_2$ | Au/carrier | | [18] |
| Titanium core/stainless steel mantle (n.d.) | – | 10 | 14 | 450 | No reaction reported | γ-$Al_2O_3$ wash coating | – | [20] |

[a] Measured temperature difference (K) within the reactor system without reaction.
[b] Screening mode; differential (D) or integral (I) mode.
[c] Number of parallel reactors or parallel microreactor channels.
[d] Measured flow deviations (%) within one reactor system.
[e] Not determined.

Table 2
Reactions with large temperature effects where the selectivity might be improved by optimization of the catalyst composition

| Reaction | $\Delta H^{\circ}_{298}$ (kJ/mol) | $T$ (°C) | Ref. |
|---|---|---|---|
| $CO + \frac{1}{2}O_2 \rightarrow CO_2$ | −283 | 150–160 | [21] |
| $H_2 + \frac{1}{2}O_2 \rightarrow H_2O$ (parallel reaction) | | | |
| $CO + 3H_2 \leftrightarrow CH_4 + H_2O$ | −210 | 180–200 | [22] |
| $NH_3 + C_2H_6 + \frac{3}{2}O_2 \rightarrow CH_3CN + 3H_2O$ | −506 | 475–500 | [23] |
| $(CH_3)_2NNH_2 + 4O_2 \rightarrow 2CO_2 + N_2 + 4H_2O$ | −1799 | 500–600 | [24] |
| $C_4H_{10} \leftrightarrow C_4H_8 + H_2$ | +126 | 700–750 | [25] |
| $CH_4 + 2H_2O \leftrightarrow 4H_2 + CO_2$ | +165 | 800–850 | [26] |
| $NH_3 + CH_4 \leftrightarrow HCN + 3H_2$ | +252 | 1100–1150 | [27] |

Table 3
Physical properties of reactor materials [32][a]

| Material | $T_{melt}$ (°C) | $\lambda$ (W m$^{-1}$ K$^{-1}$) | $E$ (GPa) | $\alpha$ ($10^{-6}$ K$^{-1}$) |
|---|---|---|---|---|
| Mo | 2620 | 138 | 315 | 5 |
| Quartz | 1607 | 0.22 | 70 | 0.4 |
| AISI 316 | 1507 | 50 | 196 | 10 |
| Ni | 1452 | 91 | 196 | 12.7 |
| Si | 1420 | 80–150 | 100–110 | 4.2 |
| Cu | 1083 | 390 | 128 | 16.8 |
| Al | 660 | 220 | 71 | 23.2 |

[a] $T_{melt}$ >1200 °C, $\lambda$ >125 W m$^{-1}$ K$^{-1}$, $E$ >150 GPa, and $\alpha$ <$10^{-5}$ K$^{-1}$ are the design criteria.

the differential mode, which considerably simplifies kinetic analysis and allows direct application of reaction kinetics in process development [33]. The catalytic layer can be deposited on the substrate by means of various techniques, such as anoxic oxidation, sol–gel synthesis, in situ growth or sputtering [34].

Based on the selected thickness of the molybdenum plates, eight rectangular shaped cavities with curved edges of 130 μm height, 400 μm width were produced along the compartment length of 40 mm by electric discharge machining (EDM) [34,35]. The electrode for machining molybdenum was in this case a 0.1 mm wire of brass, coated with zinc. In this EDM study two grades of molybdenum were tested, a molybdenum alloy containing 0.5% Ti and 0.08% Zr, and pure molybdenum (Mo 99.99+%). The former offers a considerable higher strength at temperatures above 1300 °C. Because of the additives, the EDM processing in the molybdenum alloy resulted in irregularly shaped microstructures, which contained microcracks that could affect the performance of molybdenum parts adversely if the surface is stressed in tension. However, the EDM process worked remarkably well in case of pure molybdenum, where all microstructures were produced along the length of the reactor with a tolerance below 4 μm.

Molybdenum readily starts to oxidize in air already at 300 °C at atmospheric pressure [36], which urges the need for a protective coating. Molybdenum disilicide ($MoSi_2$) is a promising material for high temperature structural applications because of its relatively high thermal conductivity and excellent oxidation resistance [37–39]. However, $MoSi_2$ disintegrates to a powder when subjected to oxidizing environments in the 400–600 °C range, which is known as the "pest" effect [40–42]. $MoSi_2$ composites might offer a possible solution for protection of molybdenum in the full temperature range [43,44].

Another possibility to protect molybdenum below 550 °C is atomic layer deposition (ALD) of a thin $Al_2O_3$ layer [45]. ALD is a coating process capable of depositing ultra-thin, conformal films of a variety of materials with atomic-level thickness control [45–48]. Recently, Groner et al. reported that the $Al_2O_3$ ALD film grows remarkably well and is an excellent choice for an insulating or protective film

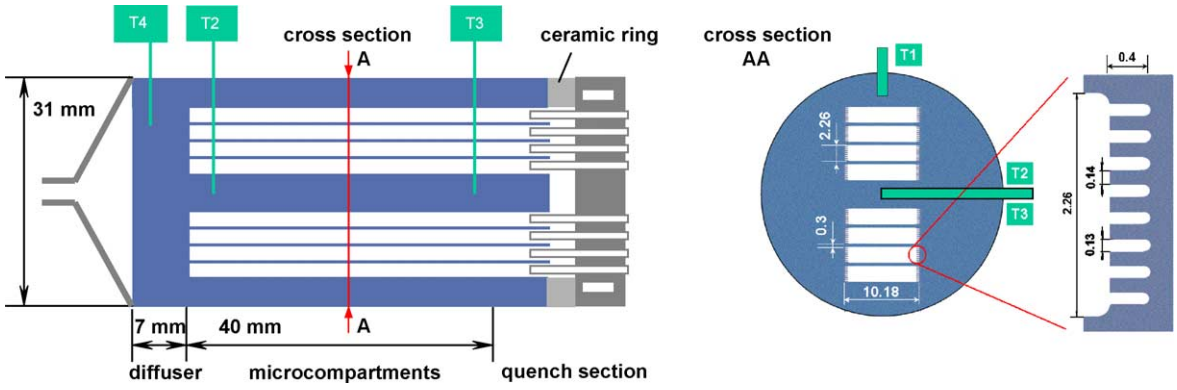


Fig. 1. Right part: layout of the high throughput microreactor. Left part: cross section of the reactor containing eight microstructured compartments. Dimensions are given in mm.

on a wide variety of substrates, including molybdenum [48].

In the present study a series of molybdenum substrates, on which $Al_2O_3$ layers were deposited up to 500 nm by ALD, were tested in air and water vapour up to 600 °C. Layer thickness and temperature are crucial parameters for the alumina layer stability. Above 550 °C the $Al_2O_3$ layers are easily detached from the molybdenum surface. Furthermore, a layer thickness of 200 nm is optimal for conditions up to 550 °C, since no mass increase could be observed, due to Mo oxide formation, in contrast to $Al_2O_3$ layers with a thickness above 300 nm, where layer destruction was observed. However, the 200 nm alumina layer remained stable, even after an exposure of 150 h at the same testing conditions.

### 2.2. HTMR layout

The HTMR consists of three separate zones, viz. the flow diffuser, the actual reactor part, and the quench section (Fig. 1). The flow diffuser is designed in a way that the inlet gas mixture is preheated to the reaction temperature and evenly distributed over the eight reactor compartments in the full flow range of 50–1000 ml/min STP (Section 3.1). Both flow inlet and reactor sections are provided with separate electrical heaters and with several temperature sensors to measure axial and radial temperature distributions (Fig. 1). In the quench section, the temperature of the outlet gases should be decreased from the reaction temperature to ca. 120 °C within a millisecond time range to avoid an extensive by-product formation downstream of the reactor (Section 3.2). The quench section is made of AISI 316 stainless steel and is separated from the hot reactor section by a 3 mm thick ceramic ring. The sampling system consists of 24 capillaries, which are positioned slightly inside the compartments to avoid cross-talking between different catalyst compositions (Section 3.3). Three capillaries per compartment are used to validate the data and to measure possible radial concentration gradients. The outlet gas composition from the separate compartments is sent to a mass spectrometer, selecting one of the sampling capillaries via a multi-positional valve system.

Actually, the main drawback of the present reactor concept is a considerable heat transfer resistance at the contact area between the individual plates and the main body of the reactor. With the present reactor design the temperature non-uniformity can be estimated, considering the case when no physical contact is realised between the molybdenum plates, containing the catalyst coating, and the reactor body. The difference between the temperature of a Mo plate and the reactor housing is estimated at a typical case when a flow of 1000 $cm^3$/min (STP) passes the reactor. The reactant concentration was assumed to be 50 mol%, $\Delta H_{298} = -500$ kJ/mol, with a conversion of 15%. In this case, the total heat ($Q$) to be transferred from the reaction zone is 28 W (64 plates) or 0.44 W per single molybdenum plate. The effective heat transfer area is the area between a single molybdenum plate and the main body of the reactor. The cross section area ($S$) is equal to $3.2 \times 10^{-5}$ $m^2$, which is four times the distance in which the plates are inserted inside the cavities ($4 \times 0.2$ mm) times the reactor length (40 mm) (Fig. 1). Furthermore, the gas thermal conductivity ($\lambda$), and the distance between a Mo plate and the wall of the microstructure ($l$) is assumed to be 0.2 W $m^{-1}$ $K^{-1}$ at 500 °C and 0.015 mm, respectively. This distance, $l$, is estimated as half the difference between cavity in the reactor wall (0.13 mm) and the thickness of a plate (0.10 mm). Substituting these values in Eq. (1), the temperature non-uniformity, $\Delta T$, between a single plate and the main reactor body can be calculated:

$$\Delta T = \frac{Ql}{S\lambda} \quad (1)$$

The temperature non-uniformity is found to be less than 1 K, which satisfies the design criterion.

## 3. High throughput microreactor simulation and design

### 3.1. Flow diffuser

In the flow diffuser, the reactant flow has to be preheated from room temperature to the reaction temperature and distributed equally throughout the microstructured compartments. The flow enters the inlet diffuser, at a typical velocity in the range of 50–1000 $cm^3$/min (STP) and it is divided in half by the symmetrical design of the inlet pipe. Therefore, only half of the complete geometry of the flow diffuser and the corresponding four reactor compartments were modelled. The geometry of the module is shown in Fig. 2. Such geometry of the flow diffuser has all the benefits of a structured design, such as improved pressure recovery due to a negligible pressure drop via the unit, and virtually clog-free behaviour, which is important for this specific application. At the same time the most critical drawback of flow diffusers, a limited flow range, is eliminated.

However, the flow has to be distributed equally in four reactor compartments. To reach this goal, the direction of the reactor compartments is shifted by a 90° turn relative to the direction of the diffuser compartments. In this way, the reagents flow in a half circular motion which causes the flow to travel in all directions (180°) at the diffuser/reactor interface and eliminates the possibility of local concentration non-uniformities or streaking, and allows the flow to be distributed appropriately in the reactor compartments. To get the uniform flow in the reactor compartments, special care has to be taken over two design parameters only ($a$ and $b$, Fig. 2). In the present design study, distance $a$ (separation) was defined as the minimum length between two adjacent reactor compartment walls. Distance $b$ was defined as a minimum length between the top wall of the reactor compartment and a side wall of a diffuser compartment.

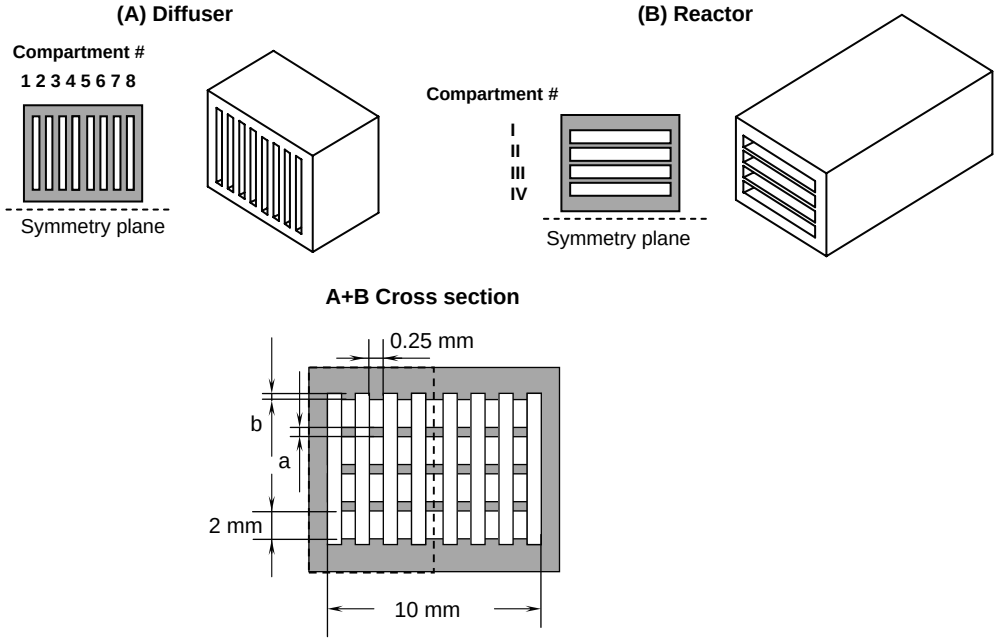


Fig. 2. Assembling of the flow diffuser and microreactor. Half of the total device is shown. The design parameters and the dimensions are indicated. The area of the numerical simulation is shown by the dashed rectangle.

The cross section of the reactor compartments was fixed at 10 mm × 2 mm based on the typical range of contact times required for catalytic coating testing (viz., 0.1–10 s). This value is slightly different from the actual value, but it was taken to facilitate grid generation. In the diffuser design, the total open area of all compartments was fixed at the value of 80 $mm^2$, which corresponds to the cross section of four reactor compartments. The equal open area in the reactor and diffuser compartments guarantees the lowest pressure drop via the device. The effect of the number of the diffuser compartments and the distance between compartments (pitch) on the flow distribution was investigated. It was found that there is no influence of these parameters on the flow distribution if the number of compartments was more than 6. However, a smaller number of diffuser compartments leads to a relatively large width of individual compartments and as a result a longer diffuser length would be required to preheat the reactant mixture. On the other hand, a large number of compartments would hamper the manufacturing of the device considerably. Therefore, we have chosen a design with eight diffuser compartments, in which all diffuser compartments have a width of 1.03 mm with a distance of 0.25 mm in between. At a fixed height of the diffuser compartments of 10 mm, a minimum diffuser length of ca. 4 and 7 mm would be required to preheat the reaction mixture to 500 and 800 °C, respectively. To satisfy the most severe case, the diffuser length was fixed at the latter value (7 mm).

Once the basic design parameters are fixed, a study was made to find the optimal *b*/*a* value. Again, due to the symmetry only half the geometry including four diffuser compartments has to be modelled. The temperature was fixed at 25 °C at the four diffuser inlets. Uniform static pressure of 101 100 Pa was specified at the four reactor outlets. The diffuser and reactor temperature were fixed at 500 °C. Physical parameters of air were used in the whole study for definition of gas phase properties. Distance *a* was fixed at 0.25 mm and the flow distribution was investigated at several different *b*/*a* ratios. At first, a uniform flow distribution was applied at the inlet of the diffuser compartments. At $b = 0$, the flow distribution was non-uniform with a maximum flow in the second and third reactor compartments. As the *b*/*a* ratio increases, more flow goes via the first and fourth reactor compartments (Fig. 3(a)). Therefore, between *b*/*a* ratios of 0.5 and 1.0, there exist an optimal value at which a uniform flow distribution can be obtained.

To characterize the degree of the flow non-uniformity, a special parameter (*s*) was introduced, defined as the mean square deviation from the average flow value:

$$s = \sqrt{\frac{\sum_{i=1}^{4}(u_i - \bar{u})^2}{3}} \tag{2}$$

where $u_i$ is the area averaged velocity in the compartment *i*. To compare the results obtained at different flow velocities, the degree of flow non-uniformity in percent from the total flow was defined as

$$\delta\,(\%) = \frac{s \times 100}{\bar{u}} \tag{3}$$

Fig. 3(b) shows that parameter $\delta$ has a minimum in the range of *b*/*a* ratios in between 0.80 and 0.83, depending on the flow velocity. At the *b*/*a* value of ca. 0.81, the mean square deviation does not exceed 0.5% for the whole range of flow velocities studied.

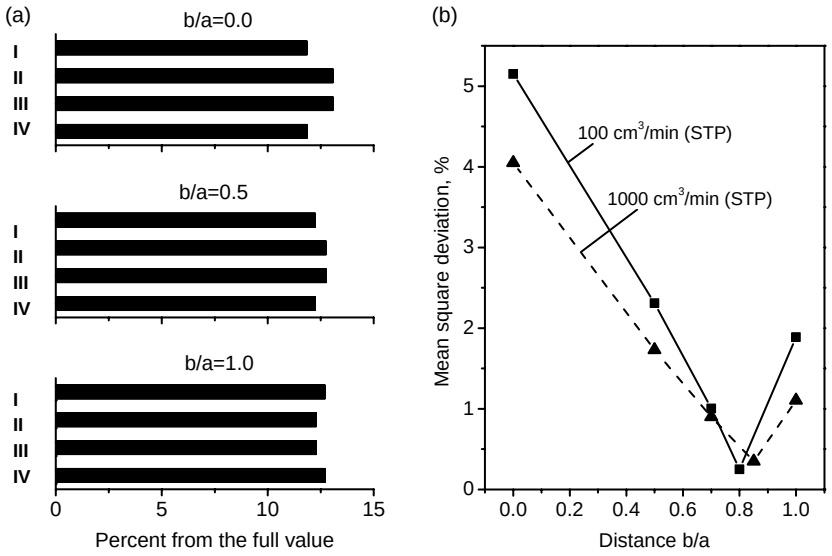


Fig. 3. (a) Flow distributions in the reactor compartments as a function of the $b/a$ ratio. (b) Mean square deviation from the average value as a function of the $b/a$ ratio at different flow velocities.

Now consider the flow distribution in the reactor compartments at a non-uniform flow distribution specified at the diffuser inlets. Actually, the typical geometry of the inlet chamber before the diffuser inlets has a conical shape providing more flow along the centreline and less near the walls. Therefore, the middle diffuser compartments would receive more flow than the outermost ones. Fig. 4 shows three flow distributions taken in the diffuser compartments by using a "standard" conical geometry of the inlet chamber: inlet tube OD of 3 mm, ID of 2 mm, chamber length of 11 mm, and the angle between the centreline and the wall of 22°. Below a flow rate of 20 $cm^3$/min (STP), the flow non-uniformity in the diffuser compartments did not exceed 1% from the average value. The flow non-uniformity increases considerably with increasing the reactant flow (Fig. 4). Deviations of 12 and 30% from the average value were obtained at a flow velocity of 100 and 1000 $cm^3$/min (STP), respectively. However, at the fixed parameters $a = 0.3$ mm and $b = 0.24$ mm, the non-uniformity in the reactor compartments calculated by Eq. (3) was 0.35 and 0.80%, respectively. Thus, the design criterion for flow non-uniformity for the diffuser of 1% is satisfied. Based on the values obtained, the height of the diffuser compartment ($h$) was fixed at

$$h = 4.6a + 4c \quad (4)$$

where $c$ is the width of the reactor compartment. This gives a height of the diffuser compartment of 10.42 mm at $a = 0.3$ mm and $c = 2.26$ mm. The estimated mechanical precision of module assembling is $5 \times 10^{-3}$ mm, which would guarantee a flow non-uniformity in the reactor compartments below 1%.

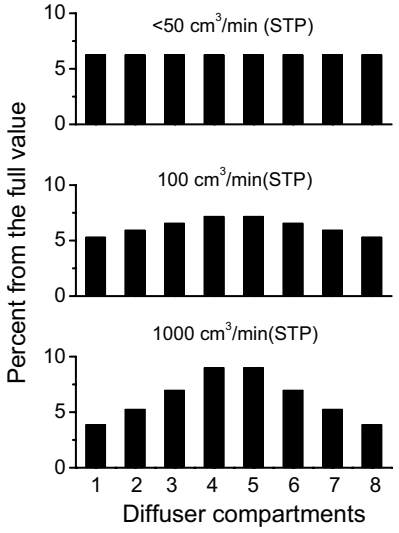


Fig. 4. Flow distributions at the entrance of the diffuser compartments at different flow velocities obtained with a conical shaped geometry of an inlet chamber. This conical chamber connects the 3 mm inlet tube with the flow diffuser. Geometry specifications—inlet tube: OD 3 mm, ID 2 mm; chamber length, 11 mm; angle between the centreline and the chamber wall, 22°.

### 3.2. Quench section

The geometry of the quench section is shown in Fig. 5. Assuming that the coolant temperature does not significantly change along the coolant chamber, a quarter of the complete unit has to be modelled. The sampling capillary inner diameter was fixed at 1.0 mm to provide a flow of ca. 1 $cm^3$/min (STP) for mass spectrometrical analysis. Three criteria were applied to the design of this unit. First of all, the temperature of the effluent gases inside the capillary should be decreased from the reactor temperature to ca. 120 °C within a millisecond time range. Secondly, the temperature

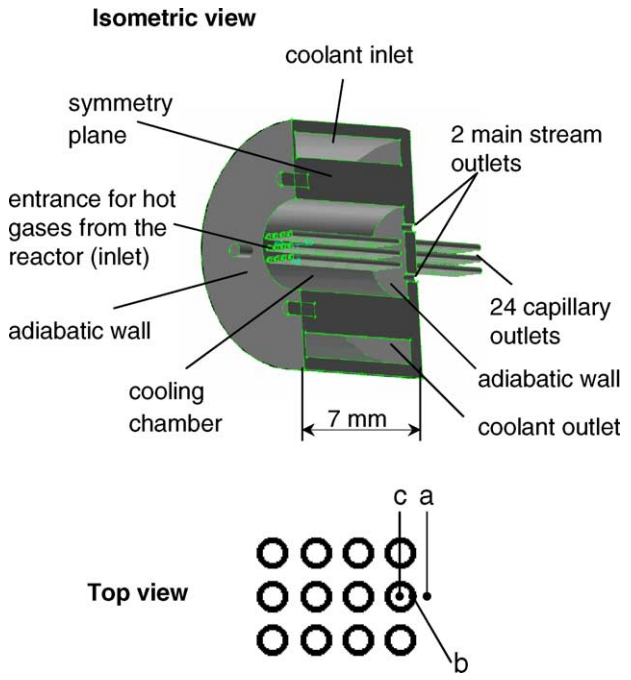


Fig. 5. Computational domain of the quench section. Points a, b, and c indicate the position at which the temperature profiles are shown in Fig. 6.

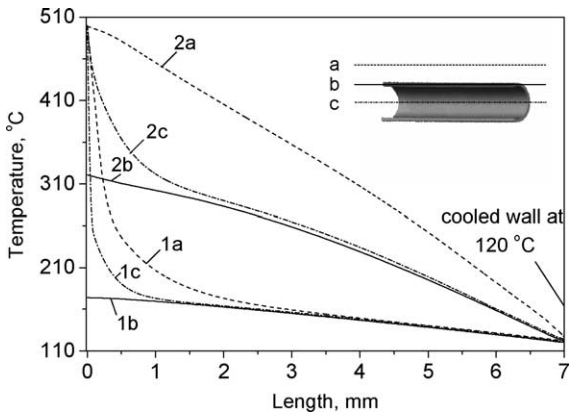


Fig. 6. Temperature profiles along the specified positions: a, inside the main stream; b, inside the capillary wall; c, along the centreline of the capillary. Main stream gas flow velocity: 1–100 $cm^3$/min (STP), 2–1000 $cm^3$/min (STP).

of the hot ends of the stainless steel capillaries should not exceed 350 °C to prevent them from oxidation/corrosion. The outer diameter of the sampling capillary defines the metal cross section and, therefore, the heat transfer rate. Finally, the temperature of the product main stream has to be decreased to ca. 150 °C to avoid damaging of the electronic valves positioned downstream of the module.

Fig. 6 demonstrates the calculated temperature profiles in the hottest part of the device—in the close vicinity of the central sample capillary (half of the actual geometry is shown). In the most severe case, having a flow velocity of 1000 $cm^3$/min (STP) and a temperature of the outlet gases of 500 °C, the temperature of the products drops to ca. 300 °C already after 3 mm in a sampling capillary with an outer diameter of 1.2 mm, corresponding to a quenching time of 0.5 ms. The temperature at the hot end of the capillary is about 320 °C, while the temperature of the main stream drops to 120 °C at the distance of 7 mm from the capillary inlet, satisfying the design criteria. If the flow velocity is fixed at its lower design value of 100 $cm^3$/min (STP), the quenching of products happens within a 1 mm distance (Fig. 6).

### 3.3. Sampling section

To make the whole unit as compact as possible, the outlets of the reactor compartment were designed at a distance of 250 μm from each other. To avoid cross-talking between the adjacent compartments, it is necessary to take samples inside the compartments [16]. In order to find a minimal distance for capillary inlets inside a compartment, a typical case was studied when a 10% oxygen in helium mixture was fed in every other compartment, while a 10% nitrogen in helium mixture was fed in the adjacent compartments. The computational domain is shown in Fig. 7 together with

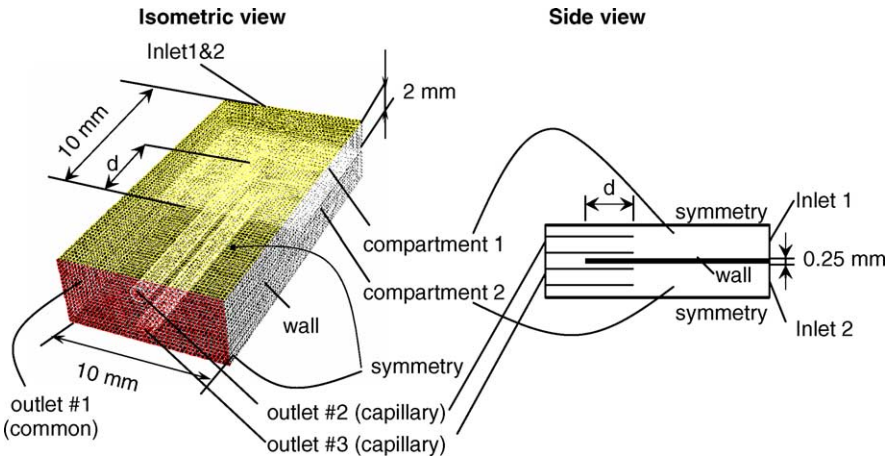


Fig. 7. Computational domain applied in the cross-talking CFD study between two adjacent compartments.

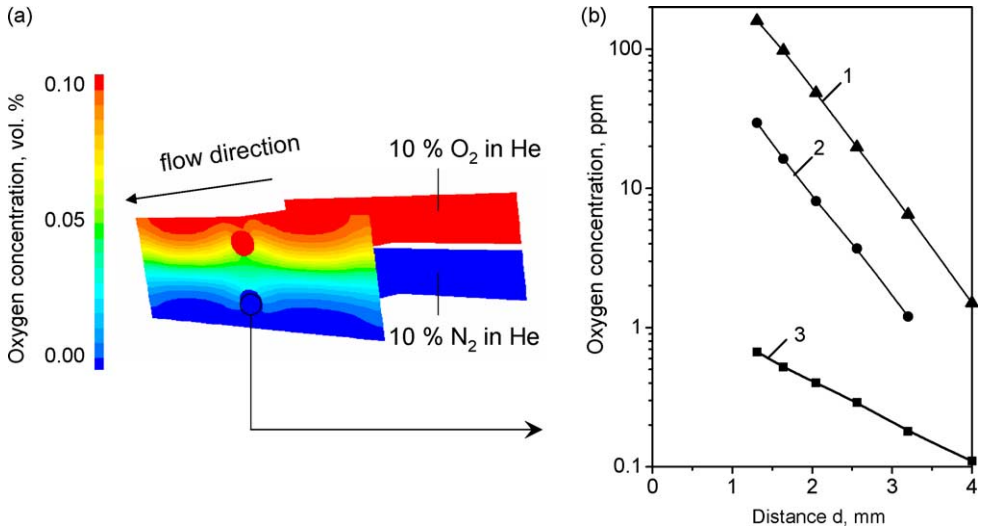


Fig. 8. (a) Oxygen concentration profile at inlet and outlet of a reactor compartment. The inlets of the sampling tubes are positioned inside the reactor compartments. Geometry specifications are given in Fig. 7. (b) Area averaged oxygen concentration at the capillary outlet #3. Total flow velocity: 1, 50 $cm^3$/min; 2, 75 $cm^3$/min; 3, 100 $cm^3$/min (STP). See Fig. 7 for definitions.

the geometry specifications. Due to the symmetry, only two adjacent compartments were modelled. Furthermore, only one capillary positioned in the centre of the compartment was considered. The linear velocity at the capillary inlet was equal to that in the main stream (iso-kinetic suction). Due to this condition, the capillary only slightly disturbs the flow and the modelling of one capillary appears to be enough. All outlets were specified as outflow regions with flow weighting factors proportional to the cross sectional area of the outlets. The latter condition was required to provide for iso-kinetic suction. Both inlets were defined as pressure inlets with a pressure drop providing the desired linear velocity of 0.02 m/s at the inlet position.

Fig. 8 shows the molar concentration of oxygen in the nitrogen flow versus the position of the capillary inlet inside the compartments (distance *d*). Oxygen concentration depends strongly on the flow rate and on the distance *d*. The minimum distance of the capillary inlet required for reliable catalyst screening at a minimum flow velocity of 12 $cm^3$/min (STP) (1/8 of the total value) is located 4 mm inside the compartment.

### 3.4. Fabrication

The high throughput microreactor has been constructed according to the present design. In Fig. 9A, a front view is presented of four compartments of the molybdenum microreactor. Fig. 9B shows half of the diffuser, which is positioned on top of the four compartments from Fig. 9A.

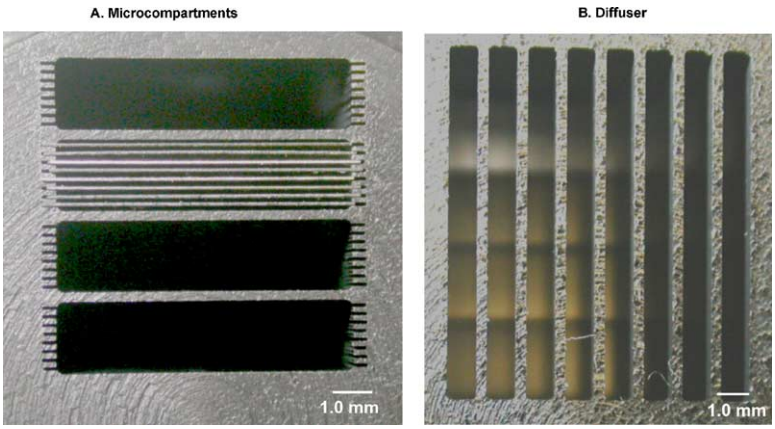


Fig. 9. The microstructured reactor fabricated by Ter Hoek Vonkerosie B.V. (The Netherlands) according to the developed design. (A) Upper four microstructured compartments. One compartment is filled with eight molybdenum plates. The microstructures have dimensions of 130 μm height and 400 μm width along the length of the compartment of 40 mm. (B) Upper half of the flow diffuser (dimensions: width, 1.03 mm; length, 10.42 mm).

## 4. Conclusion

A novel molybdenum-based high throughput microreactor has been designed for screening and optimization of catalytic coatings in high temperature reactions involving high heat effects. By proper choice of reactor material and geometry near-isothermal conditions can be realized.

A low-pressure drop flow diffuser has been designed for application in a wide flow range of 50–1000 $cm^3$/min (STP). The unique geometry of the diffuser is able to evenly distribute the flow over all reactor compartments of the HTMR, and simultaneously preheat the reactants to reaction temperatures up to 800 °C. A sampling/quench capillary system is designed to quench the effluent flow within a millisecond time range to avoid possible non-catalytic reactions downstream of the reactor. Cross-talking of product gases between different compartments was eliminated by appropriate positioning of the sampling capillaries slightly inside the compartments.

The feasibility of micromachining of molybdenum and the performance of molybdenum in corrosive environments was investigated. It was found that the presence of minor impurities, which can improve the physical properties of molybdenum, has a negative influence on the microstructures when electric discharge machining was applied. However, micromachining of pure molybdenum (99.99+%) was reproducible with tolerances below 4 μm.

The corrosion resistance of molybdenum was considerably improved by deposition of a 200 nm $Al_2O_3$ layer by means of atomic layer deposition. No significant mass increase could be observed due to oxidation after an exposure of 150 h at 550 °C in an oxidative environment.

## Acknowledgements

The financial support by the Dutch Technology Foundation (STW, project no. EPC.5543), Shell International Chemicals B.V., Akzo Nobel Chemicals B.V., and Avantium Technologies B.V. is gratefully acknowledged. The authors would also like to thank Dr. Elizaveta Vainonen-Ahlgren from ASM Microchemistry Ltd. (Finland) for her co-operation and for providing us the opportunity to apply ALD techniques.

## Appendix A

The area-averaged values of the gas velocity, $u_i$, are computed in every compartment from the results of the simulation as follows:

$$u_i = \frac{\int_{b_1}^{b_2}\int_{a_1}^{a_2} u \,\mathrm{d}x\,\mathrm{d}y}{\int_{b_1}^{b_2}\int_{a_1}^{a_2} \mathrm{d}x\,\mathrm{d}y}$$

where $b_2 - b_1$ is the height of a compartment ($2 \times 10^{-3}$ and $1 \times 10^{-2}$ m for the reactor and diffuser compartments, respectively) and $a_2 - a_1$ the width of a compartment ($1 \times 10^{-2}$, $1.03 \times 10^{-3}$ m for the reactor and diffuser compartments, respectively).

## References

[1] V. Murphy, A.F. Volpe Jr., W.H. Weinberg, Curr. Opin. Chem. Biol. 7 (2003) 427.
[2] J. Pérez-Ramírez, R.J. Berger, G. Mul, F. Kapteijn, J.A. Moulijn, Catal. Today 60 (2000) 93.
[3] J.A. Moulijn, J. Pérez-Ramírez, R.J. Berger, G. Hamminga, G. Mul, F. Kapteijn, Catal. Today 81 (2003) 457.
[4] F. Kapteijn, L. Singoredjo, N.J.J. Dekker, J.A. Moulijn, Ind. Eng. Chem. Res. 32 (1993) 445.
[5] C. Hoffmann, A. Wolf, F. Schüth, Angew. Chem. Ed. 38 (1999) 2800.
[6] C. Hoffmann, H.W. Schmidt, F. Schüth, J. Catal. 198 (2001) 348.
[7] P. Pantu, G.R. Gavalas, AIChE J. 48 (2002) 815.
[8] I. Hahndorf, O. Buyevskaya, M. Langpape, G. Grubert, S. Kolf, E. Guillon, M. Baerns, Chem. Eng. J. 89 (2002) 119.
[9] U. Rodemerck, P. Ignaszewski, M. Lucas, P. Claus, Chem. Eng. Technol. 23 (2000) 413.
[10] U. Rodemerck, P. Ignaszewski, M. Lucas, P. Claus, M. Baerns, Parallel synthesis and testing of heterogeneous catalysts, in: Proceedings of the Third International Conference on Microreaction Technology, Germany, 1999, p. 260.
[11] U. Rodemerck, D. Wolf, O.V. Buyevskaya, P. Claus, S. Senkan, M. Baerns, Chem. Eng. J. 82 (2001) 3.
[12] S. Senkan, Angew. Chem. Int. Ed. 40 (2001) 312.
[13] S.M. Senkan, Nature 394 (1998) 350.
[14] S. Senkan, K. Kranz, S. Ozturk, V. Zengin, I. Onal, Angew. Chem. Int. Ed. 38 (1999) 2794.
[15] K. Kranz, S. Ozturk, S. Senkan, Catal. Today 62 (2000) 281.
[16] T. Zech, D. Hönicke, Efficient and reliable screening of catalysts for microchannel reactors by combinatorial methods, in: Proceedings of the Fourth International Conference on Microreaction Technology, Atlanta, GA, USA, 2000, p. 379.
[17] T. Zech, D. Hönicke, A. Lohf, K. Golbig, T. Richter, Simultaneous screening of catalysts in microchannels: methodology and experimental setup, in: Proceedings of the Third International Conference on Microreaction Technology, Germany, 1999, p. 260.
[18] P. Claus, D. Hönicke, T. Zech, Catal. Today 67 (2001) 319.
[19] U. Rodemerck, P. Ignaszewski, M. Lucas, P. Claus, M. Baerns, Top. Catal. 13 (2000) 249.
[20] G. Kolb, V. Cominos, K. Drese, V. Hessel, C. Hofmann, H. Löwe, O. Wörz, R. Zaph, A novel catalyst testing microreactor for heterogeneous gas phase reactions, in: Proceedings of the Sixth International Conference on Microreaction Technology, New Orleans, LA, 2002, p. 61.
[21] Ch. Song, Catal. Today 77 (2002) 17.
[22] R. Westerholm, L.J. Pettersson, State of the art: multi-fuel reformers for automotive fuel cell applications, Problem identification and research needs, KFB-Kommunikationsforskningsberedningen, Stockholm, 1999.
[23] Y. Li, J.N. Armor, J. Catal. 173 (1998) 511.
[24] Z.R. Ismagilov, M.A. Kerzhentsev, I.Z. Ismagilov, V.A. Sazonov, V.N. Parmon, G.L. Elizarova, O.P. Pestunova, V.A. Shandakov, Yu.L. Zuev, V.N. Eryomin, N.V. Pestereva, F. Garin, H.J. Veringa, Catal. Today 75 (2002) 277.
[25] B.M. Weckhuysen, R.A. Schoonheydt, Catal. Today 51 (1999) 223.
[26] J.N. Armor, Appl. Catal. A 176 (1999) 159.
[27] M. Stroebe, V.H. Hoffmann, A. Zogg, M. Scheringer, K. Hungerbühler, Chimia 55 (2001) 887.

[28] E.V. Rebrov, M.H.J.M. de Croon, J.C. Schouten, Catal. Today 69 (2001) 183.
[29] G. Groppi, W. Ibashi, E. Tronconi, P. Forzatti, Chem. Eng. J. 82 (2001) 57.
[30] E. Tronconi, G. Groppi, Chem. Eng. J. 55 (2000) 6021.
[31] G. Groppi, G. Airoldi, C. Cristiani, E. Tronconi, Catal. Today 60 (2000) 57.
[32] R.H. Perry, D.W. Green, J.O. Maloney (Eds.), Perry's Chemical Engineers' Handbook, 7th ed., McGraw-Hill, New York, 1997.
[33] S.K. Ajmera, C. Delattre, M.A. Schmidt, K.F. Jensen, Sens. Actuators B 82 (2002) 297.
[34] A. Gavriilidis, P. Angeli, E. Cao, K. Yeong, Y.S.S. Wan, Trans. IchemE 80 (2002) 3.
[35] H. Löwe, W. Ehrfeld, Elecrochim. Acta 44 (1999) 3679.
[36] E. Best, I. Hinz, K. Swars (Eds.), Gmelin Handbook of Inorganic Chemistry, Molybdenum, Supplement Volume A3, 8th ed., Springer-Verlag, New York, 1983.
[37] K.S. Kumar, C.T. Liu, JOM 45 (1993) 28.
[38] A.K. Vasudeva, J.J. Petrovic, Mater. Sci. Eng. A 155 (1992) 1.
[39] J.J. Petrovic, A.K. Vasudevan, Mater. Res. Soc. Symp. Proc. 322 (1994) 3.
[40] T.C. Chou, T.G. Nieh, JOM 45 (1993) 214.
[41] T.C. Chou, T.G. Nieh, Scripta Met. Et. Mat. 26 (1992) 1637.
[42] T.C. Chou, T.G. Nieh, Scripta Met. Et. Mat. 27 (1992) 19.
[43] T. Maruyama, K. Yanagihara, Mater. Sci. Eng. A 239 (1997) 828.
[44] K. Natesan, S.C. Deevi, Intermettalics 8 (2000) 1147.
[45] R. Matero, M. Ritala, M. Leskela, T. Salo, J. Aromaa, O. Forsen, Phys. IV France 9 (1999) 493.
[46] E. Vainonen-Ahlgren, E. Tois, T. Ahlgren, L. Khriachtchev, J. Marles, S. Haukka, M. Tuominen, Comput. Mater. Sci. 27 (2003) 65.
[47] N.D. Hoivik, J.W. Elam, R.J. Linderman, V.M. Bright, S.M. George, Y.C. Lee, Sens. Actuators A 103 (2003) 100.
[48] M.D. Groner, J.W. Elam, F.H. Fabreguette, S.M. George, Thin Solid Films 413 (2002) 186.